Geoscience Letters

RESEARCH LETTER

Open Access

Added value of high-resolution regional climate model in simulating precipitation based on the changes in kinetic energy

Gayoung Kim[1,2], Jineun Kim[3] and Dong-Hyun Cha[1*]

Abstract

As the resolution of regional climate models has increased with the development of computing resources, Added Values (AVs) have always been a steady research topic. Most previous studies examined AVs qualitatively by comparing model results with different model resolutions qualitatively. This study tried to quantitatively investigate the AV of the high-resolution regional climate model for precipitation by analyzing the distribution of kinetic energy according to the different wavelengths at two different resolutions (36 km vs. 4 km), away from the traditional comparative analysis. In addition, the experiment that the low-resolution topography was forced to the high-resolution model was additionally conducted to separate the AVs associated with the topographic effect. Among the three experiments, two with the same topography and two with the exact horizontal resolution were compared separately. With identical topography, the high-resolution model simulated amplified precipitation intensity more than the low-resolution model in all quantiles, especially for extreme precipitation. The precipitation generated by mesoscale or smaller scale weather/climate events was also simulated with greater intensity in the high-resolution model. With the same grid spacing, the more detailed topography model showed AV for increasing spatial variability of precipitation, especially in mountainous regions. The AVs identified in this study were related to kinetic energy with wavelengths at the meso-beta or smaller scale. On the other hand, the kinetic energy above the meso-alpha or larger scale has no significant correlation with the AV of precipitation.

Keywords: Regional climate model, Added Value, Horizontal resolution, Kinetic energy

Introduction

Due to climate change, natural disasters are becoming more intense and frequent and commonly cause severe damage (Coronese et al. 2019; Madsen et al. 2014; Otto et al. 2018; Van Aalst 2006). Moreover, as global warming intensifies, numerous studies have predicted increased summer precipitation in East Asia (Kim et al. 2018; Lee and Cha 2020; Park et al. 2021). Hence, advanced precipitation forecasting technologies are essential for the management of these coming disasters, because East Asia is particularly vulnerable to precipitation-related disasters due to many megacities with more than 10 million inhabitants situated along the coast, as well as the combination of complex topography and various meteorological phenomena (Hong and Kanamitsu 2014; Lee et al. 2017; Liu et al. 2017; Son et al. 2017). The development of high-performance computing resources has made it possible to simulate the earth system at high resolution. In the 1970s, the general circulation model (GCM) with a coarse resolution of 2.5° ~ 10° was used for climate prediction (Manabe et al. 1970; Wellck et al. 1971). Recently, however, climate simulations have become possible using a GCM with a resolution of less than 1° (Kim et al. 2019; Sakamoto et al. 2012; Werner et al. 2011). Even in the

*Correspondence: dhcha@unist.ac.kr

[1] School of Urban and Environmental Engineering, Ulsan National Institute of Science & Technology (UNIST), 50 UNIST-gil, Ulju-gun, Ulsan 689-798, Republic of Korea
Full list of author information is available at the end of the article

High Resolution Model Intercomparison Project (HighResMIP), an inter-comparison project of GCM simulation results at high resolution, the global climate was reproduced with a spatial resolution of up to 25 km. The results of this climate simulation were evaluated to serve as a more reliable source for assessing climate risks (Ajibola et al. 2020; Haarsma et al. 2016, 2020). Meanwhile, a regional climate model (RCM) was developed in the late 1980s, allowing efficient high-resolution simulation of a specific region using the dynamic downscaling method (Giorgi 1990). In the early stage of RCM development, many studies were conducted using the RCM with a resolution of at least 60 km (Giorgi et al. 1990; Mearns et al. 1995). The RCM has also developed with computing technology, making it possible to conduct multi-decadal simulations at a very high resolution (Berg et al. 2019; Cha et al. 2016; Fantini et al. 2018; Kim et al. 2018). In particular, studies have been actively conducted using convection-permitting models (CPMs), the current state-of-the-art models with very high-resolution (usually < 4 km) which can directly simulate deep-convective processes without convection parameterizations (Clark et al. 2016; Lenderink et al. 2021; Meredith et al. 2020; Prein et al. 2015).

As model resolutions have improved, the added value (AV) gained from using a high-resolution model over a coarser-resolution model has been constantly emphasized. A typical example of AV is that high-resolution models are particularly good at simulating extreme precipitation (Kopparla et al. 2013; Lim et al. 2014; Park et al. 2020; Rauscher et al. 2016; Shi et al. 2018; Tölle et al. 2018; Torma et al. 2015; Vichot-Llano et al. 2021). For example, Fumière et al. (2020) showed that simulated hourly precipitation extremes in France were significantly improved when the horizontal resolution was enhanced. In addition, as the resolution was improved, the model performance for simulating weather events at the mesoscale or local horizontal scale (e.g., tropical cyclone, mesoscale convective system) could be improved (Jang and Hong 2014; Jin et al. 2014; Johnson et al. 2013; Lee et al. 2020; Uddin et al. 2021). Another benefit of high-resolution models is that topography can be expressed in greater detail, improving the spatial correlation between modeled and observed precipitation (Güttler et al. 2015; Li et al. 2015; Pontoppidan et al. 2017; Smith et al. 2015; Tselioudis et al. 2012), especially in mountainous regions, such as the Alps (Torma et al. 2015). However, there are also disadvantages to using high-resolution models. In some cases, precipitation was overestimated as the grid spacing decreased (Li et al. 2020; Tripathi and Dominguez 2013). In addition, the high-resolution RCM may amplify the systematic bias of forcing data (Xu et al. 2018). Research on the positive and negative effects of high-resolution models should continue to improve weather/climate predictions using numerical models.

There are also several limitations when analyzing AVs by comparing models with different resolutions. First, the uncertainty inevitably arises when forcibly converting the grid of one experiment into another to express AVs spatially. Hence, most previous studies have demonstrated that the high-resolution models improve the spatial distribution of the weather elements through a simple qualitative comparison without damaging the raw model data (Gibba et al. 2019; Giorgi 2019; Lucas-Picher et al. 2021). However, the qualitative comparisons can create a visual optical illusion which leads to misinterpretations. Another limitation is that the simple comparison with observation cannot sufficiently explain the dynamic/physical processes for a specific AV. In other words, it is difficult to know whether the differences between the model experiments with dissimilar resolutions are caused by AVs or amplified noise. Therefore, various analysis methods are needed to more quantitatively investigate AVs of a high-resolution model and to understand associated processes.

This study was conducted based on many of the studies mentioned above, in which weather/climate event at a small horizontal scale is more reasonably simulated as the grid spacing decreases. However, this study tried to quantitatively estimate AVs using spectral analysis, away from the traditional analysis technique. It was assumed that as the resolution improved, kinetic energy with a relatively short wavelength would increase when a weather event on a small-scale occurred. This study examined the influence of low-level (850 hPa) kinetic energy with various wavelengths on the AV of the simulated precipitation with high resolution for the Korean Peninsula. This study was accomplished by comparing two experiments with different model resolutions. This paper is organized in the following manner: model configuration, experimental design, and analytical methods are introduced in "Data and methods" section. "Results" section presents the results for the AV of simulated precipitation with high resolution. Finally, the summary and conclusions are given in "Summary and conclusions" section.

Data and methods

Model configuration and experimental design

We used the Advanced Research WRF (ARW) model, version 4.1.2. The initial and boundary conditions were obtained from the ERA-Interim reanalysis data set with a spatial and temporal resolution of 0.7° and 6 h. The model consisted of three domains with horizontal grid spacings of 36 km (d01, 277 × 173), 12 km (d02, 262 × 220), and 4 km (d03, 214 × 214), and the target area was focused on the Korean Peninsula (Fig. 1a). We used

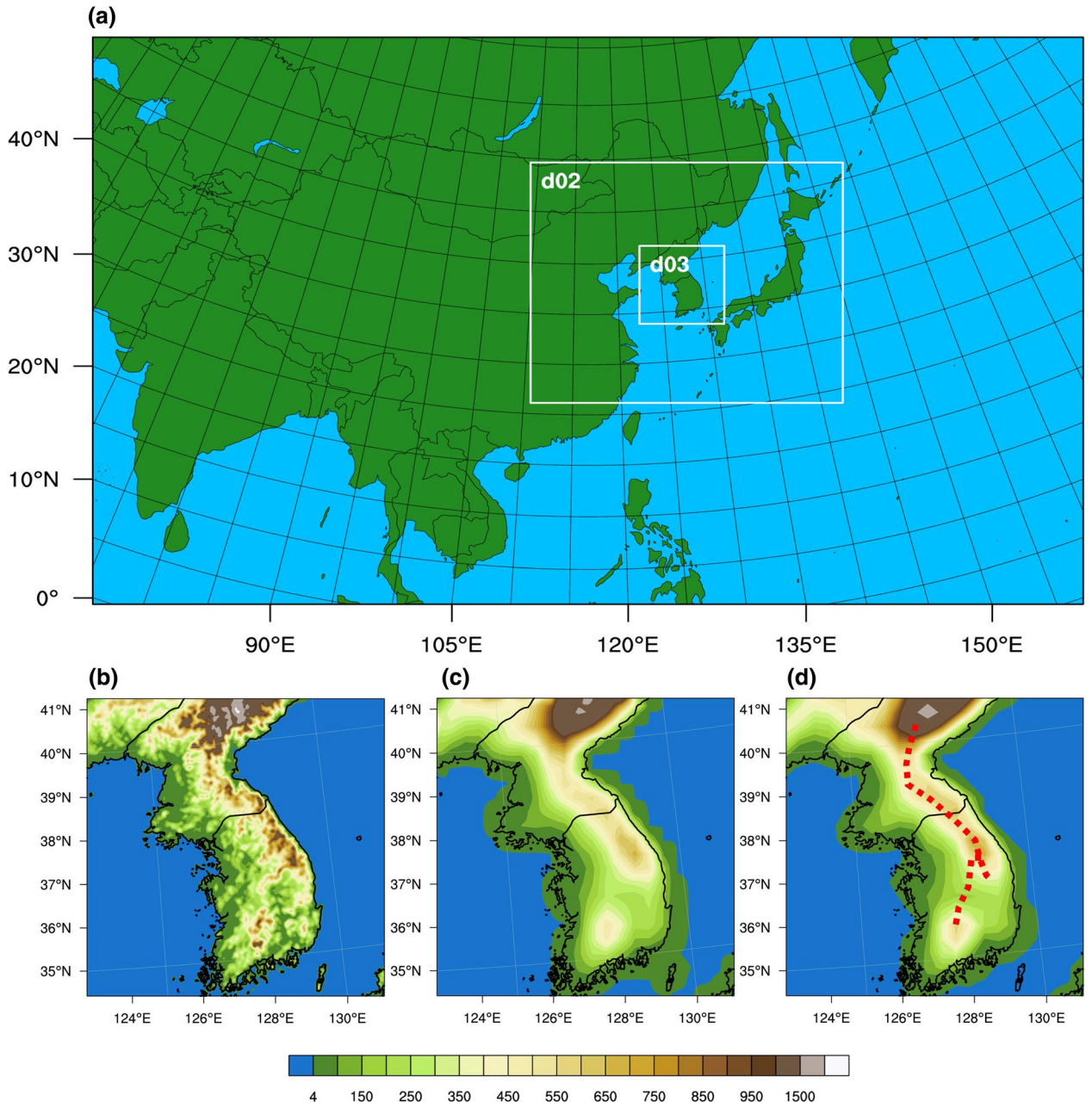

Fig. 1 **a** WRF model domains with two nests and **b**–**d** topography (m) of the innermost domain in CTRL04, LOW04, and CTRL36, respectively. The dashed red lines indicate the mountainous areas

one-way nested domains with a Lambert conformal map projection. There were 33 hybrid levels from the surface to 50 hPa vertically. The physics options configured in the model included the Yonsei University planetary boundary layer scheme (Hong et al. 2006), the WRF single-moment six-class graupel microphysics scheme (Hong and Lim 2006), the multi-scale Kain–Fritsch cumulus parameterization (Zheng et al. 2016), the Rapid Radiative Transfer Model for general circulation models (Iacono et al. 2008), the Mesoscale Model version 5 Monin–Obukhov surface layer scheme (Jiménez et al. 2012), and the Noah land surface model (Chen and Dudhia 2001). The simulation period was set from 0000 UTC on 1st May to 0000 UTC on 1st September 2001, 2006, 2009,

and 2011. The experimental years were selected based on the year in which noteworthy extreme precipitation events occurred in South Korea after 2000 (KMA 2012). The first month was used as the spin-up period. The sea-surface temperatures were updated at 6-h intervals using the ERA-Interim data set. In addition, the spectral nudging technique (Cha et al. 2011; Miguez-Macho et al. 2004; Moon et al. 2018; von Storch et al. 2000) was applied to the zonal and meridional wind components in the outermost domain to constrain the model to be more consistent with the ERA-Interim data set. The wind components with wavelengths longer than 1000 km were nudged.

As the grid spacing decreases, the topography changes, so the actual resolution effect includes the changed topographic effect. Hence, two experiments were performed to investigate the impacts of the horizontal resolution on the precipitation simulation, isolating the different topography effects: (1) a control experiment (CTRL) with no topography change, (2) the same experiment as CTRL except for lower resolution topography (LOW). The topography in the CTRL experiments was obtained from the Global Multi-resolution Terrain Elevation Data 2010 (GTMED2010) with a horizontal resolution of 5 arc-minutes in d01 and d02 and 30 arc-seconds in d03. In the LOW experiment, the topography of the innermost domain was replaced with that of the outermost domain using bilinear interpolation (Fig. 1b–d). Here, CTRL36 (same as LOW36) indicates the results for the outermost domain of the CTRL experiment, while CTRL04 and LOW04 indicate the results for the innermost domains. The low-resolution topography data tended to lower topography and its deviation, especially in the eastern part of the Korean Peninsula, consisting of mountainous areas. The maximum difference in topography height between the high-resolution and low-resolution data was about 800 m.

We used 95 stations of the Automated Synoptic Observing System (ASOS) data in South Korea to verify the simulated precipitation. Each model data was interpolated on a curvilinear grid to an unstructured grid of ASOS using the bilinear interpolation method and then verified.

Analytical methods

Based on the prior studies mentioned above, we hypothesized that higher model resolution could result in (1) greater extreme precipitation intensity, (2) increased short-duration precipitation due to smaller scale weather events, and (3) increased orographic precipitation. To evaluate these hypotheses, the impacts of the grid spacing on (1) the precipitation intensity and (2) the size of the rain cell were compared between the two experiments with the same topography (CTRL36 vs. LOW04). For this analysis, the results of the outermost domain were cropped to the area of the innermost domain. In addition, the effect of the different topographies on (3) the spatial distribution of simulated precipitation was compared between two experiments with the same grid spacing (CTRL04 vs. LOW04). The daily precipitation was extracted for analysis if it exceeded 1 $mm \cdot day^{-1}$. Hereafter, the AVs by a higher resolution model with fixed topography (LOW04) and those by an identical resolution model with more detailed topography (CTRL04) are referred to as the "fine-mesh effect" and the "detailed topographic effect," respectively.

We calculated the sizes of 3-hourly rain cells during all simulation periods to examine the relationship between model resolution and simulated precipitation events with a short duration induced by small-scale weather phenomena. In this study, the rain cells were defined as the closed contours over which rainfall intensity exceeded 0.1 mm for 3 h. Figure 2 shows an example of how to identify and group rain cells. Rain cells were calculated at every output interval (i.e., 3 h), so every rain cell is two-dimensional. It is determined whether or not to assign a numbering of the rain cell group at each calculating grid moving eastward and northward (see Fig. 2c). The procedure of the rain cell grouping at each calculating grid is as follows. First, if the precipitation exceeds the threshold (0.1 mm) at the calculating grid, the rain cell group number is assigned sequentially, starting 1 by comparing four surrounding grids. It is noted that only four of eight surrounding grids need to be checked (see comparing grids in Fig. 2c), because we checked each grid in the order of eastward and northward directions. A new number is assigned if there is no grid, where the precipitation exceeds the threshold among the comparing grids. However, if just one comparing grid exceeds the threshold, the group number of corresponding comparing grids is assigned to the calculating grid. In addition, if two or more cells exceed the threshold, the smallest group number among the comparing cells is assigned to the calculating cell, and the group number of all comparing cells is also changed to the same number (see group 1 in Fig. 2c). This procedure makes it possible to quantify the size of the rain cell.

This study used the spectral method to examine the model performance for kinetic energy depending on model resolution (Castro et al. 2005) and its association with simulated precipitation in the three hypotheses mentioned above. We used kinetic energy at

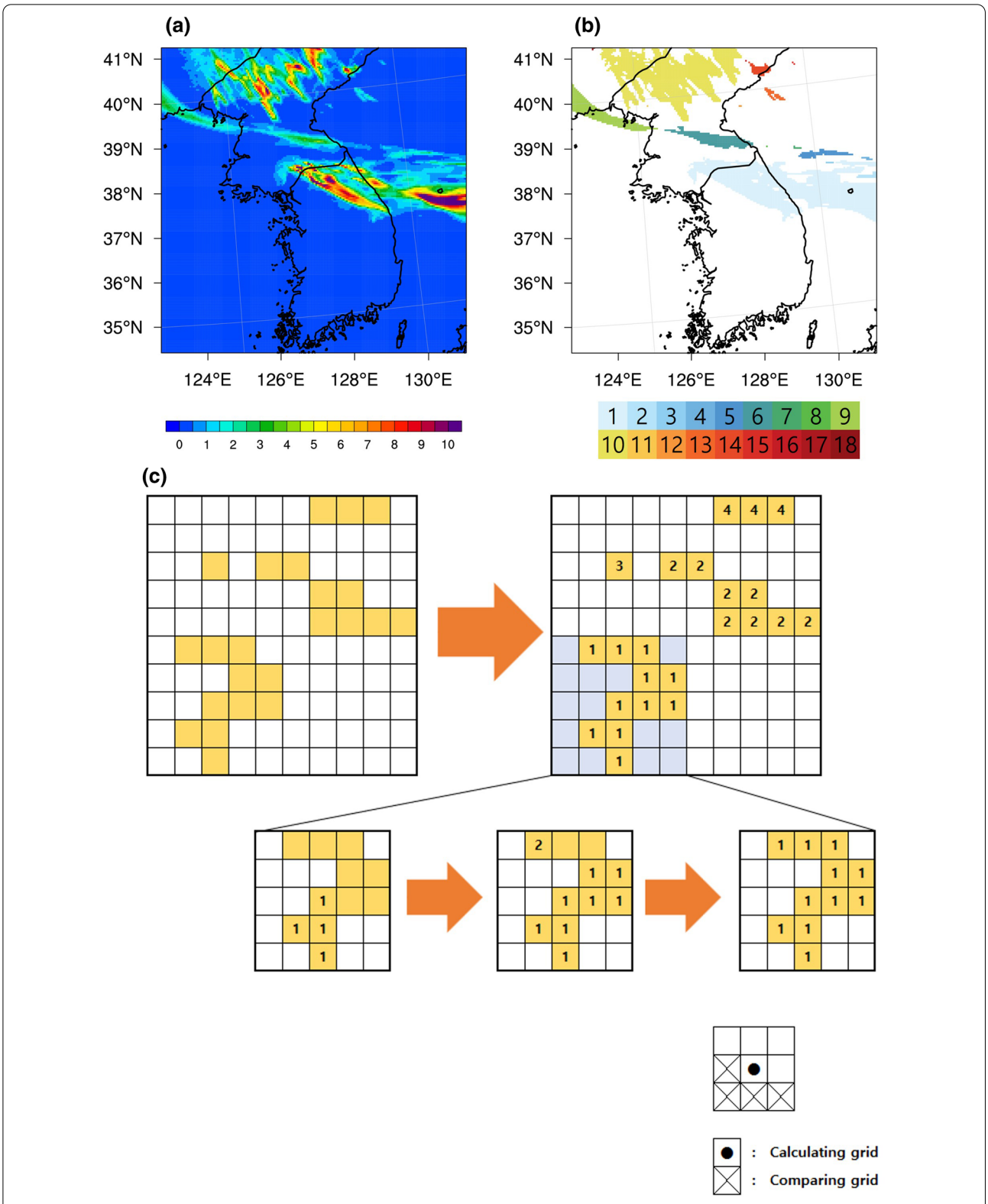

Fig. 2 **a** Snapshot of 3-hourly precipitation, **b** corresponding result of the rain cell grouping, and **c** illustration of rain cell grouping algorithm

850 hPa (TOTAL), which showed the highest temporal correlation with precipitation at various vertical levels (not shown). In this study, the kinetic energy was calculated as follows:

$$\mathrm{TOTAL}\left(\mathrm{m^2 s^{-2}}\right) = 0.5 \cdot \left(\mathrm{ua850^2} + \mathrm{va850^2}\right) \quad (1)$$

where ua850 and va850 indicate the zonal and meridional wind components at 850 hPa. We obtained the kinetic energy spectrum at different wavelengths following the method of Skamarock (2004) and Bolgiani et al. (2020) (Fig. 3a–c). Due to the limited domain sizes, the model in the target area (innermost domain) can simulate weather/climate events ranging from meso-α to meso-γ scales (Orlanski 1975). In this study, the TOTAL within the target area was filtered based on a wavelength of 200 km, which was the boundary between meso-α and meso-β scales, using the spectral method. The wind components with wavelengths longer (shorter) than 200 km were extracted as $\mathrm{ua850_{GE200}}$ and $\mathrm{va850_{GE200}}$ ($\mathrm{ua850_{LT200}}$ and $\mathrm{va850_{LT200}}$). The kinetic energies for the new wind components with wavelengths of meso-α (WMA) and meso-β (WMB) scales were then obtained as follows:

$$\mathrm{WMA}\left(\mathrm{m^2 s^{-2}}\right) = 0.5 \cdot \left(\mathrm{ua850_{GE200^2}} + \mathrm{va850_{GE200^2}}\right) \quad (2)$$

$$\mathrm{WMB}\left(\mathrm{m^2 s^{-2}}\right) = 0.5 \cdot \left(\mathrm{ua850_{LT200^2}} + \mathrm{va850_{LT200^2}}\right) \quad (3)$$

Using WMA and WMB, we analyzed the relationship between decomposed kinetic energy and simulated precipitation at different model resolutions.

Results

Validation of precipitation

Although it is difficult to verify the high-resolution model data, because the resolution of observation has not kept up with those of models, it is still necessary to give the observed rainfall pattern as a general benchmark for verifying the model performance. Thus, the spatial patterns of seasonal (JJA) mean precipitation between observation and each model data were compared in 95 stations (Fig. 4). In the case of the low-resolution model (CTRL36), precipitation was underestimated in most regions, especially in some parts of the northwestern and Southern regions of South Korea. However, when the model resolution was higher (CTRL04 and LOW04), the negative biases were greatly reduced, although they did not improve significantly in spatial distribution. When detailed topographic data were used (CTRL04), the bias pattern was similar to that of LOW04 but showed slight differences depending on the region. Although CTRL04 slightly overestimated precipitation in the mountainous eastern part of South Korea, it decreased mean biases by increasing overall precipitation compared to LOW04.

Fine-mesh effects

Prior to the analysis of precipitation intensity, the time series of differences in area-averaged daily precipitation and energy spectrum (i.e., WMA and WMB) between CTRL36 and LOW04 were analyzed to examine the general relationship between simulated precipitation and kinetic energy, as well as the changes in the relationship depending on the model resolution (Fig. 5). As the resolution increased, precipitation, WMA, and WMB increased on most days. The variation in precipitation

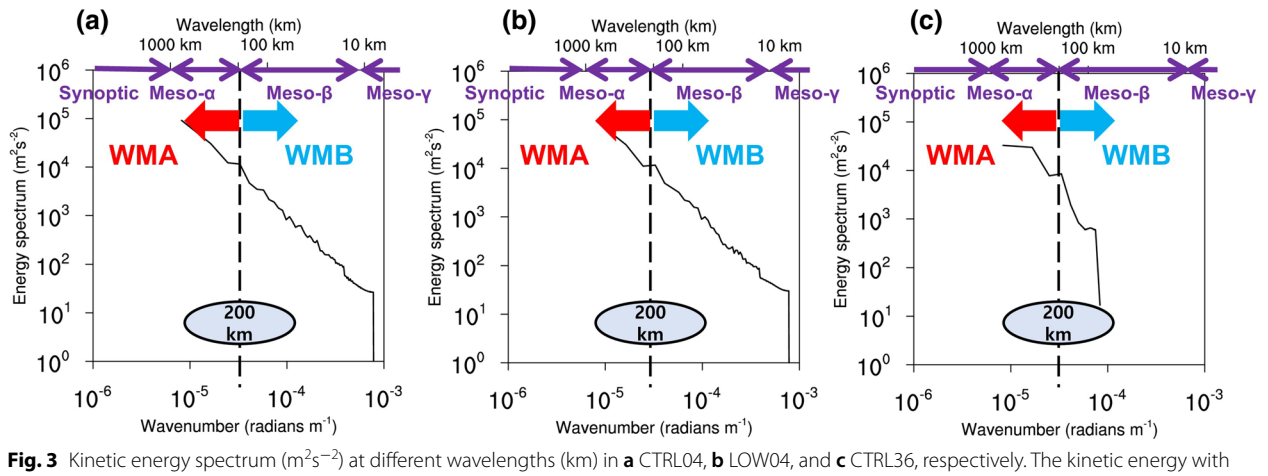

Fig. 3 Kinetic energy spectrum ($\mathrm{m^2 s^{-2}}$) at different wavelengths (km) in **a** CTRL04, **b** LOW04, and **c** CTRL36, respectively. The kinetic energy with wavelengths longer (shorter) than 200 km is indicated by WMA (WMB)

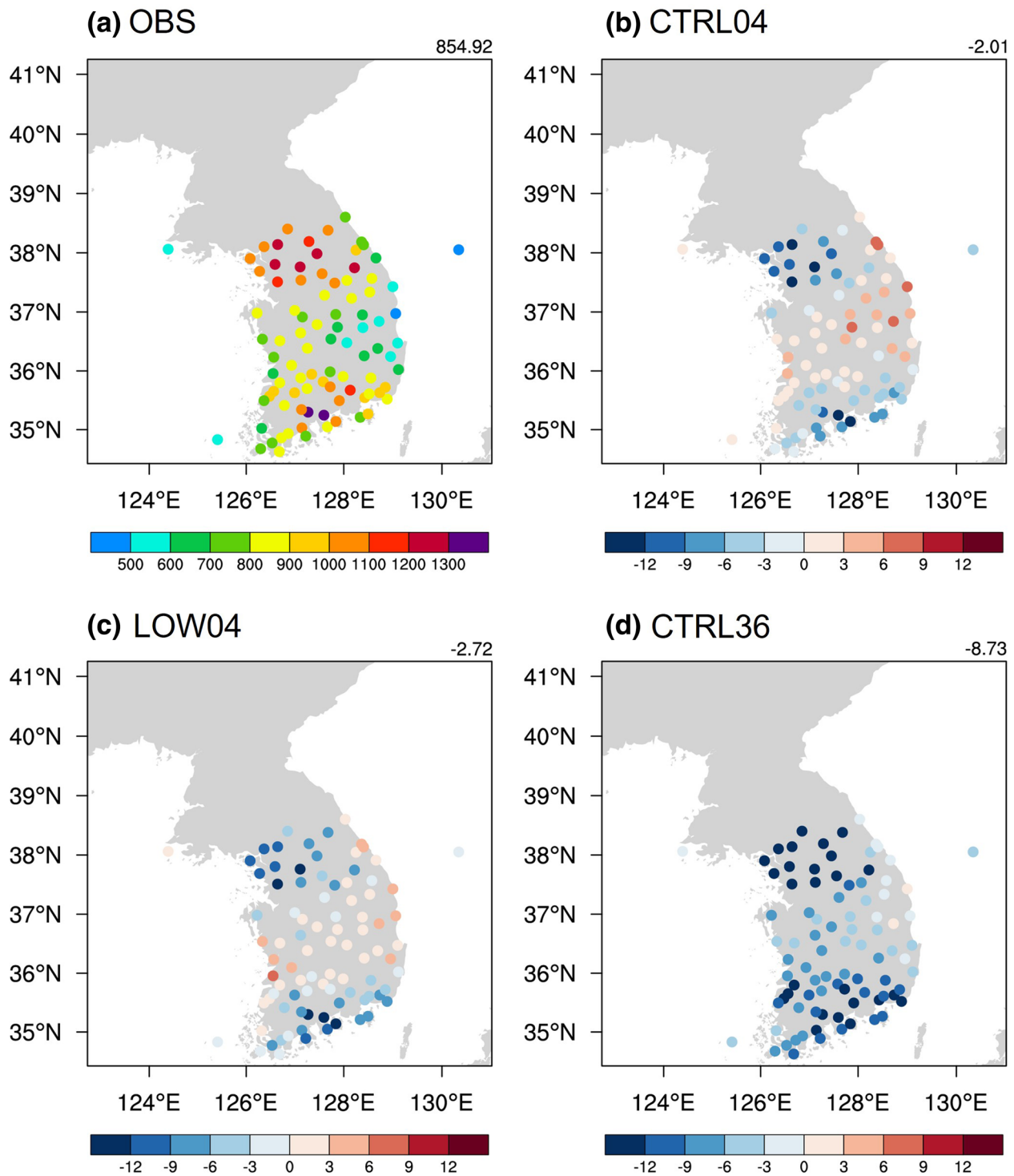

Fig. 4 Summer (June to August) mean precipitation (mm) during experimental period for **a** ASOS, and its biases (mm) for **b** CTRL04, **c** LOW04, and **d** CTRL36, respectively. The mean values of the biases are written on the top-right of each panel

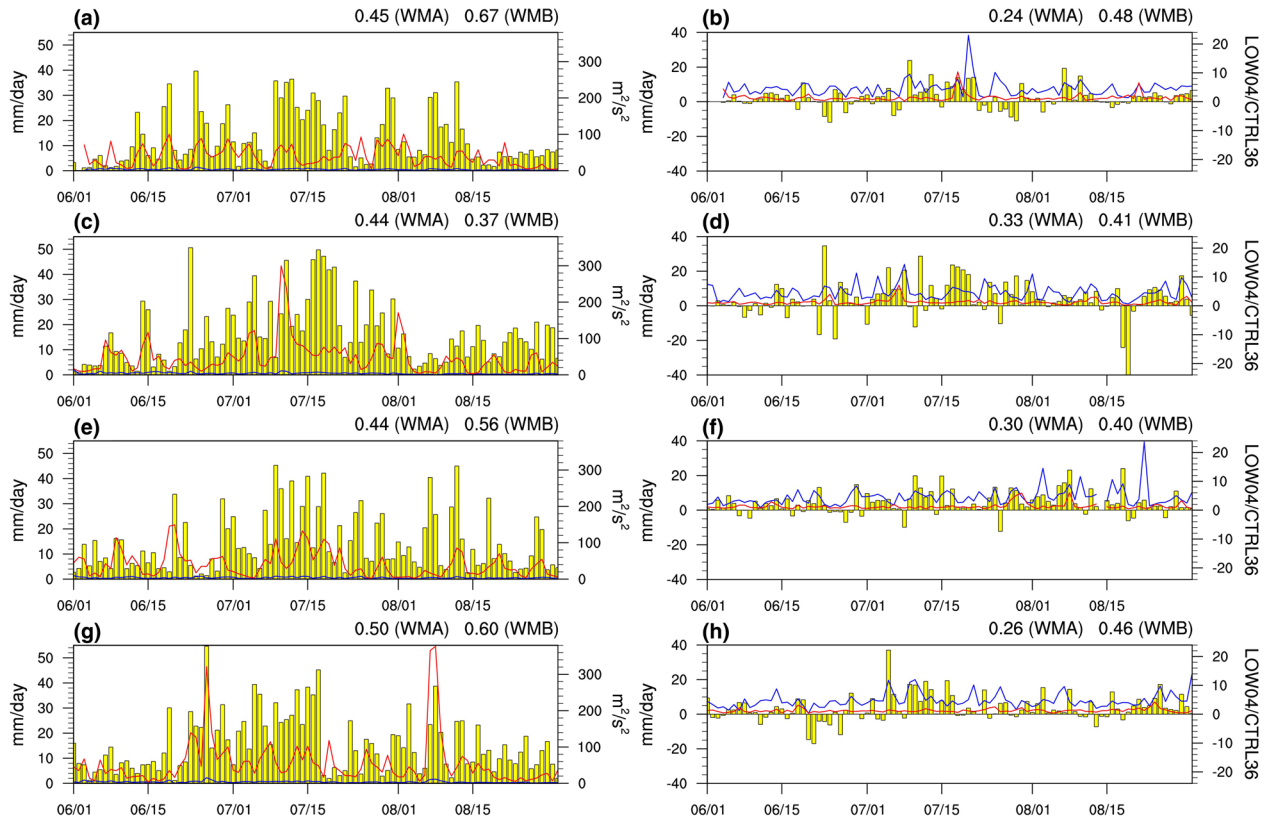

Fig. 5 Area-averaged daily precipitation and kinetic energy of LOW04 (left) and their changes compared to CTRL36 (right) for **a**, **b** 2001, **c**, **d** 2006, **e**, **f** 2009, and **g**, **h** 2011; yellow bar, red line, and blue line represent the precipitation (mm·day^{-1}), WMA [m^2·s^{-2} (left) ratio (right)], and WMB [m^2·s^{-2} (left) ratio (right)], respectively. The temporal correlation coefficients between precipitation and kinetic energy are written on the top-right of each panel

Table 1 Changes in daily precipitation (mm·day^{-1}) and kinetic energy (m^2·s^{-2}) between LOW04 and CTRL36 with their significances (*p* value) calculated from *t* test

	2001	2006	2009	2011
Precipitation	2.3 (0.13)	**3.9 (0.02)***	**4.1 (0.01)***	**3.5 (0.03)***
WMA	3.8 (0.35)	1.6 (0.82)	0.7 (0.90)	5.7 (0.52)
WMB	**2.3 (0.00)***	**3.1 (0.00)***	**2.7 (0.00)***	**2.9 (0.00)***

The values in bold with stars are statistical significance at 90% level

and WMB with different model resolutions was significant in most years; however, it was not significant in the case of WMA. As the model resolution was higher, mean WMB (WMA) increased by 4.57 times (1.31 times) when the mean precipitation increased by 3.47 mm·day^{-1}. Likewise, the *t* test results demonstrated significant changes in precipitation and WMB but not in WMA (Table 1). In other words, the difference in precipitation simulated by models with different resolutions could be more relevant to WMB than WMA. Moreover, the precipitation is more correlated temporally to WMB than WMA, especially in 2001 and 2011. Despite the small magnitude of WMB compared to WMA, WMB could be a significant driver of the difference in precipitation between the two simulations with different grid spacings. Decreasing grid spacing resulted in increased precipitation caused by smaller scale weather/climate events.

We then analyzed whether the general relations between daily precipitation and WMB could also be applied to extreme precipitation (Fig. 6). We aggregated spatial-mean daily precipitation, WMA, and WMB and then classified them into 5 groups depending on their quantiles. The light, intermediate, and extreme precipitation belonged to the two leftmost quantiles (80–100%), two middle quantiles (20–60%), and the rightmost quantile (0–20%), respectively. The difference in precipitation intensity between different grid spacings tended to increase as the quantiles decreased, which meant that extreme precipitation intensities were more enhanced at high resolution. However, WMA did not exhibit much variation in resolution

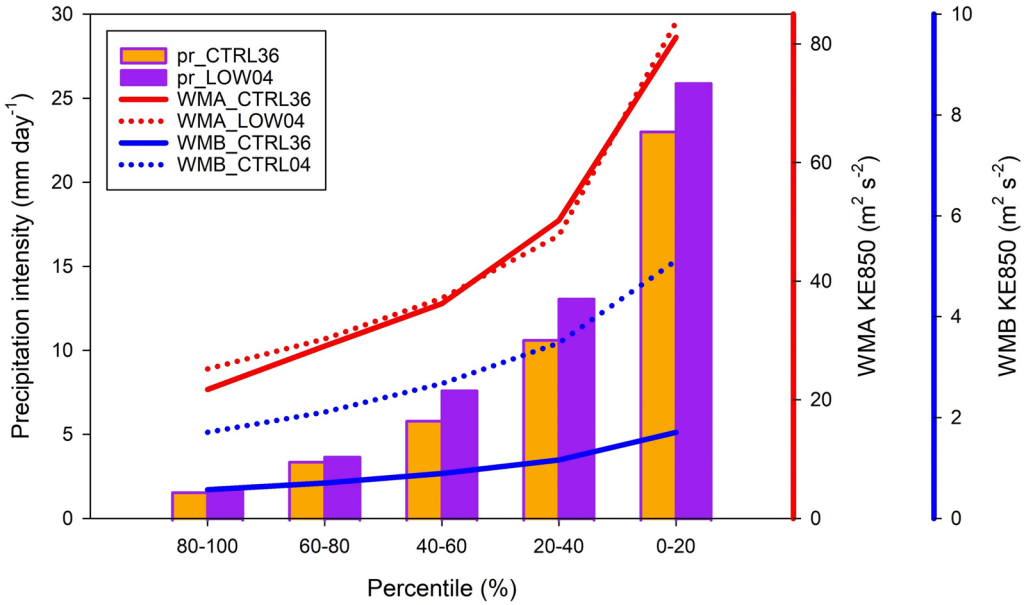

Fig. 6 Variation of precipitation intensities across different quantiles. The colored bars represent the intensity of simulated precipitation (mm·day^{-1}) for each quantile; red and blue lines indicate the results of WMA (m^2·s^{-2}) and WMB (m^2·s^{-2}), while solid and dashed lines indicate CTRL36 and LOW04

Table 2 Changes in the intensity of simulated precipitation (mm·day^{-1}) between LOW04 and CTRL36 for each quantile, and corresponding kinetic energy (m^2·s^{-2}) with their significance (*p* value) calculated from *t* test

	80–100%	60–80%	40–60%	20–40%	0–20%
Precipitation	0.1 (0.18)	**0.3 (0.02)***	**1.8 (0.00)***	**2.4 (0.00)***	**2.9 (0.08)***
WMA	3.5 (0.36)	1.2 (0.76)	0.9 (0.86)	− 2.5 (0.68)	2.5 (0.82)
WMB	**1.2 (0.00)***	**1.5 (0.00)***	**2.0 (0.00)***	**2.6 (0.00)***	**3.7 (0.00)***

The values in bold with stars are statistical significance at 90% level

across all quantiles, suggesting that varying precipitation intensities between different model resolutions were irrelevant for WMA. However, high-resolution WMBs at all quantiles were higher than low-resolution ones, especially at upper quantiles (i.e., higher precipitation intensity and larger WMB). The *t* test results in Table 2 proved the significance of the variation in precipitation and WMB with different model resolutions. Figure 3 shows that WMB could drive the phenomenon of increased precipitation at a higher resolution, especially extreme precipitation.

Earlier results indicated that higher resolution models increased simulated precipitation due to WMB rather than WMA. Because WMB has a shorter wavelength, it could induce intense precipitation in limited areas. Hence, the next step was to explore how models with different resolutions simulated precipitation intensity based on rain cell sizes (Fig. 7). Here, after rain cells in all simulations were aggregated, they were divided into 8 groups according to the size of the rain cell. It is noted that the size threshold was set to 36^2 km^2 considering the grid spacing of the low-resolution model (CTRL36). Two experiments exhibited significant differences in the simulated spatial deviation, average, and maximum precipitation intensity of rain cells with a small size ranging to 400^2 km^2. The higher resolution model reproduced higher intensities of both mean and extreme precipitation of small-scale precipitation than the lower resolution one. In addition, the LOW04 simulated high spatial deviation of rain cells with relatively small size, which indicated intensities of small-scale precipitation were higher than the CTRL36. Meanwhile, in rain cells with a large size of 400^2 km^2 or more, the differences between model results decreased as the size increased. Considering that the range of the meso-β (meso-α) scale was 20–200 km (200–2000 km), as shown in Fig. 3, the differences in the performance for the precipitation simulation depending on the grid spacing occurred in the meso-β and part of the meso-α scale. This AV was considered to be correlated with kinetic energy, as shown in previous results. WMA showed a different pattern to precipitation. Compared to WMB, the impact of grid spacing on WMA was negligible, but the differences in WMA between experiments were

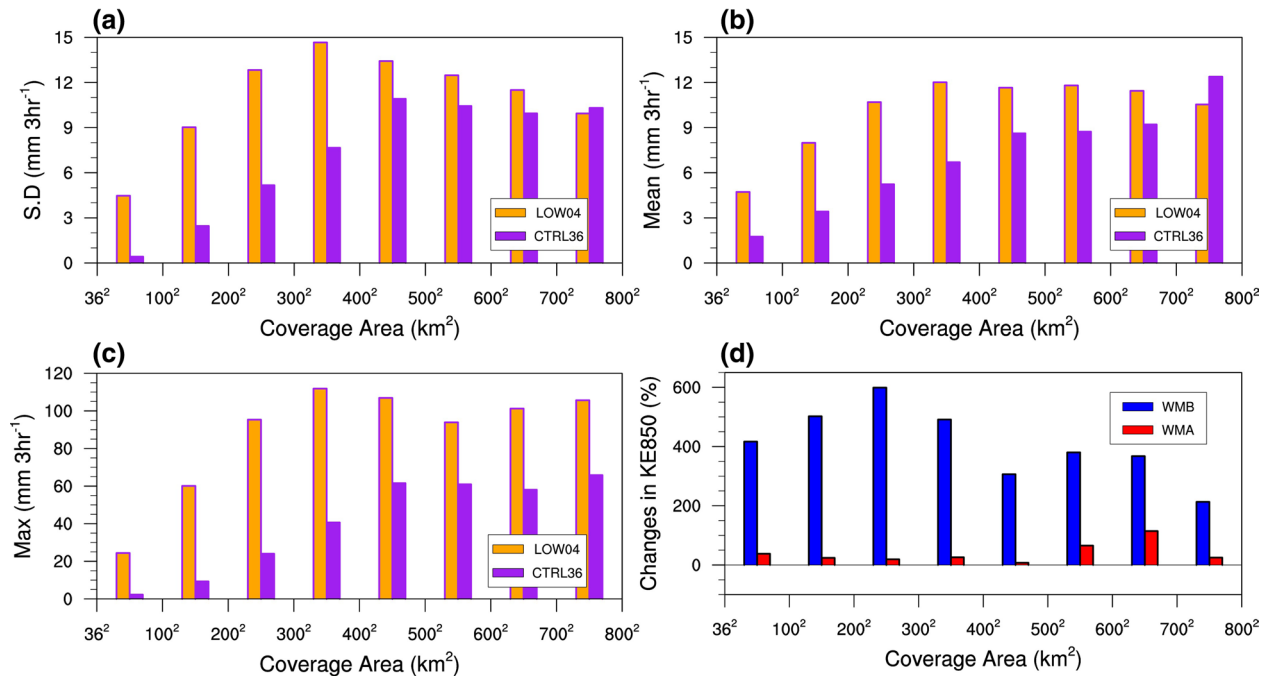

Fig. 7 Variation in precipitation intensities based on the size of the rain cell: **a**–**c** standard deviation, average, and maximum precipitation intensities, respectively, for each rain cell on a 3-hourly scale (mm·3 h^{-1}). **d** Changes in WMA and WMB of LOW04 compared to CTRL36 (%)

prominent when the size of the rain cell was more expansive. However, WMB showed a pattern similar to precipitation; the values obtained from the models with different resolutions exhibited significant differences when the rain cells had a small size. As the grid spacing decreased, the model simulated smaller scale precipitation caused by more WMB.

Detailed topographic effects

Two experiments were conducted with the same grid spacing but different topography to analyze the impact of the detailed topography on precipitation simulation (Fig. 8). Compared to LOW04, CTRL04 could express more detailed topography, especially in the mountainous regions located in the eastern region of the Korean Peninsula (see also Fig. 1b, c). In LOW04, the ranges of terrain

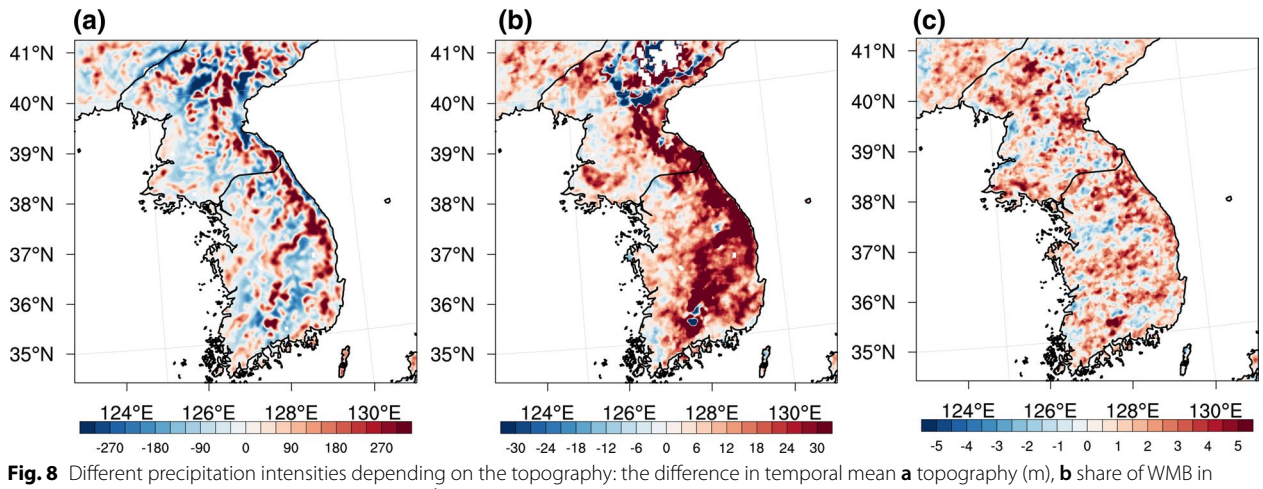

Fig. 8 Different precipitation intensities depending on the topography: the difference in temporal mean **a** topography (m), **b** share of WMB in TOTAL (%), and **c** precipitation intensity (mm·day^{-1}) between CTRL04 and LOW04

height in the mountainous regions were 500–700 m, whereas CTRL04 expressed the height of 800–1000 m, close to the actual topography. The changed topography affected the simulation of kinetic energy. The changes in the proportion of WMB in the total kinetic energy increased markedly in mountainous areas. In addition, regions of increased precipitation were primarily consistent with those of increased WMB. As with denser grid spacing, detailed topography increased WMB, which induced small-scale precipitation caused by orographic lifting.

More quantitative analysis was conducted to ensure relationships among topography, precipitation, WMA, and WMB (Fig. 9). We classified daily precipitation, WMA, and WMB into 5 groups depending on the topographic height. In the rightmost quantile (0–20%), which has the highest elevation, precipitation of CTRL04 was significantly greater than that of LOW04. However, there was no significant change in precipitation between the two experiments in other quantiles. Most of the increased precipitation in CTRL04 occurred at high altitudes. WMA tended to decrease as the altitude increased in both experiments, and there was little significant difference between the two experiments. Hence, it is hard to correlate precipitation increment at high altitudes with WMA. However, the WMB of CTRL04 was significantly higher than that of LOW04 in the rightmost quantile, consistent with Table 3. The increase of WMB at high altitudes could drive increasing precipitation in CTRL04.

Summary and conclusions

This study proved that simulated precipitation on the Korean Peninsula varied depending on the horizontal resolution (36 km vs. 4 km). In addition, in this study, we attempted to evaluate AVs using spectral analysis quantitatively. We classified kinetic energy into WMA and WMB based on a wavelength threshold of 200 km and investigated which one induced more significant changes in simulated precipitation as the horizontal resolution increased. In addition, because the topography was affected by the change in model resolution, we analyzed

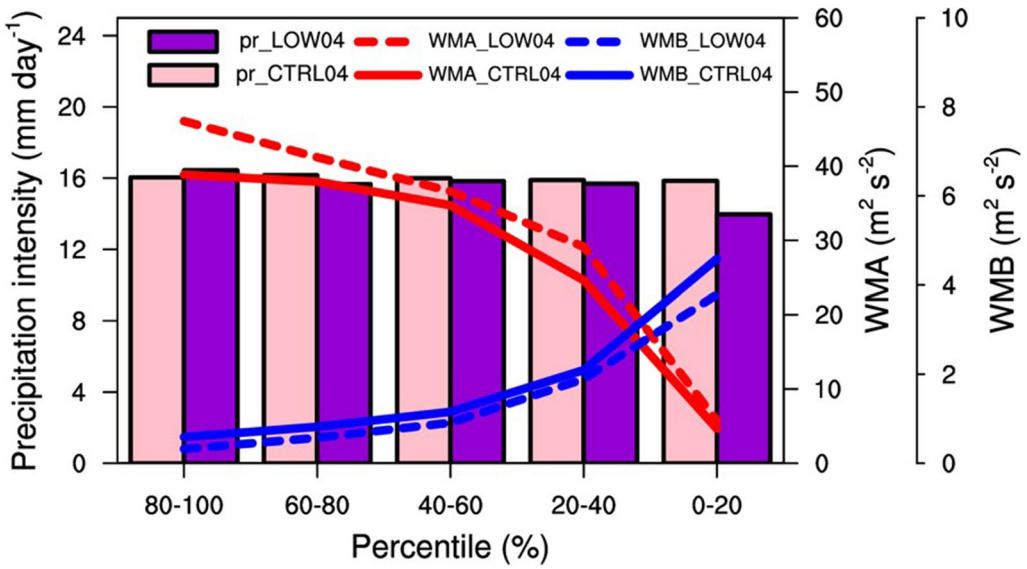

Fig. 9 Precipitation intensities (bar graph, mm·day^{-1}), WMA (red line, m^2·s^{-2}), and WMB (blue line, m^2·s^{-2}) of CTRL04 and LOW04 depending on different quantiles of topographic height (%)

Table 3 Changes in the intensity of simulated precipitation (mm·day^{-1}) between CTRL04 and LOW04 for each quantile of topography, and corresponding kinetic energy (m^2·s^{-2}) with their significance (*p* value) calculated from *t* test

	80–100%	60–80%	40–60%	20–40%	0–20%
Precipitation	0.04 (0.97)	0.86 (0.42)	0.96 (0.38)	0.45 (0.68)	**1.84 (0.07)***
WMA	− 4.29 (0.24)	− 2.01 (0.56)	− 1.17 (0.71)	− 2.75 (0.30)	− 0.53 (0.76)
WMB	0.13 (0.51)	0.26 (0.14)	0.26 (0.11)	0.22 (0.33)	**0.74 (0.02)***

The values in bold with stars are statistical significance at 90% level

the fine-mesh effect after fixing the topography at two different resolutions. We also analyzed the detailed topographic effect by fixing the grid spacing for two different topographic resolutions. With the same topography, decreased grid spacing increased in extreme precipitation intensities. Furthermore, the mean and maximum precipitation intensity for small rain cells increased. Analysis of the detailed topographic effect showed that the precipitation in mountainous areas increased when the high-resolution topography data were used, although the grid spacing was the same. The fine-mesh and detailed topographic effects all induced an increase in precipitation. The increased precipitation caused by higher resolution was not significantly related to kinetic energy at the meso-α or larger scale. However, the simulated kinetic energy at the meso-β or smaller scale significantly affected the changes in precipitation simulated by models of different resolutions. As the model resolution was enhanced, the simulated precipitation induced by weather/climate events on a meso-β or smaller scale increased. In addition, even if only the topography was detailed, while the model resolution was fixed, precipitation in the mountainous region at high altitudes induced by WMB (i.e., orographic lifting) increased.

As advancements in computing resources make it possible to conduct simulations with higher and higher resolutions, the impact of the model resolution should be investigated continuously. Especially, since summer precipitation in East Asia appears in mixed results of meteorological phenomena on various scales (e.g., monsoon on the synoptic scale, MCS on the mesoscale, and orographic effect on the regional scale), the Korean Peninsula is a place worth investigating AVs. This study emphasized that a high-resolution model should be used if the weather/climate to be analyzed has a small horizontal scale. Conversely, high-resolution models are not necessary if the analysis is conducted at a sufficiently large scale. Thus, the AV identified in this study, which refers to enhanced precipitation for small-scale weather/climate events in a high-resolution model, can be applied in a micrometeorological field, such as analyzing urban climate.

In this study, only the effects of the horizontal resolution were considered, but a few studies revealed that vertical resolution also greatly affected precipitation simulation (Liang et al. 2022; Ma et al. 2012; Volosciuk et al. 2015). Hence, it is necessary to apply the methodology of this study to investigate the sensitivity of the vertical resolution. In addition, one limitation of this study is that it was difficult to verify the model performance for kinetic energy, because there was no high-resolution reanalysis data that covered the whole analysis region. Furthermore, the experimental design was limited to a particular domain size, target area, and model resolution, making it difficult to conduct experiments under various conditions. In future research, the results of this study should be generalized to expand the experimental matrix. The disadvantages of increased model resolution should also be examined.

Author contributions

GK organized and wrote the manuscript, and JK and DHC revised it. All the authors read and approved the final manuscript.

Funding

This work was funded by the Korea Meteorological Administration Research and Development 467 Program under Grant KMI (KMI2020-01412).

Availability of data and materials

Not applicable.

Declarations

Competing interests

The authors declare that they have no competing interests.

Author details

[1]School of Urban and Environmental Engineering, Ulsan National Institute of Science & Technology (UNIST), 50 UNIST-gil, Ulju-gun, Ulsan 689-798, Republic of Korea. [2]Citizen Happiness Research Division, Ulsan Research Institute, Ulsan, Republic of Korea. [3]Disaster Prevention Research Division, National Disaster Management Research Institute, Ulsan, Republic of Korea.

Received: 22 March 2022 Accepted: 23 September 2022
Published online: 07 October 2022

References

Ajibola FO, Zhou B, TchalimGnitou G, Onyejuruwa A (2020) Evaluation of the performance of CMIP6 HighResMIP on West African precipitation. Atmosphere 11(10):1053

Berg P, Christensen OB, Klehmet K, Lenderink G, Olsson J, Teichmann C, Yang W (2019) Summertime precipitation extremes in a EURO-CORDEX 011 ensemble at an hourly resolution. Nat Hazards Earth Syst Sci 19(4):957–971

Bolgiani P, Santos-Muñoz D, Fernández-González S, Sastre M, Valero F, Martín ML (2020) Microburst detection with the WRF model Effective resolution and forecasting indices. J Geophys Res Atmos 125(14):e2020JD02883

Castro CL, Pielke RA, Leoncini G (2005) Dynamical downscaling: assessment of value retained and added using the regional atmospheric modeling system (RAMS). J Geophys Res Atmos. https://doi.org/10.1029/2004JD004721

Cha DH, Jin CS, Lee DK, Kuo YH (2011) Impact of intermittent spectral nudging on regional climate simulation using weather research and forecasting model. J Geophys Res Atmos. https://doi.org/10.1029/2010JD015069

Cha D-H, Lee D-K, Jin C-S, Kim G, Choi Y, Suh M-S, Ahn J-B, Hong S-Y, Min S-K, Park S-C (2016) Future changes in summer precipitation in regional climate simulations over the Korean Peninsula forced by multi-RCP scenarios of HadGEM2-AO. Asia Pac J Atmos Sci 52(2):139–149

Chen F, Dudhia J (2001) Coupling an advanced land surface–hydrology model with the Penn State–NCAR MM5 modeling system. Part I: model implementation and sensitivity. Month Weather Rev 129(4):569–585

Clark P, Roberts N, Lean H, Ballard SP, Charlton-Perez C (2016) Convection-permitting models: a step-change in rainfall forecasting. Meteorol Appl 23(2):165–181

Coronese M, Lamperti F, Keller K, Chiaromonte F, Roventini A (2019) Evidence for sharp increase in the economic damages of extreme natural disasters. Proc Natl Acad Sci 116(43):21450–21455

Fantini A, Raffaele F, Torma C, Bacer S, Coppola E, Giorgi F, Ahrens B, Dubois C, Sanchez E, Verdecchia M (2018) Assessment of multiple daily precipitation statistics in ERA-Interim driven Med-CORDEX and EURO-CORDEX experiments against high resolution observations. Clim Dyn 51(3):877–900
Fumière Q, Déqué M, Nuissier O, Somot S, Alias A, Caillaud C, Laurantin O, Seity Y (2020) Extreme rainfall in Mediterranean France during the fall: added value of the CNRM-AROME Convection-Permitting Regional Climate Model. Clim Dyn 55(1):77–91
Gibba P, Sylla MB, Okogbue EC, Gaye AT, Nikiema M, Kebe I (2019) State-of-the-art climate modeling of extreme precipitation over Africa: analysis of CORDEX added-value over CMIP5. Theoret Appl Climatol 137(1):1041–1057
Giorgi F (1990) Simulation of regional climate using a limited area model nested in a general circulation model. J Clim 3(9):941–963
Giorgi F (2019) Thirty years of regional climate modeling: where are we and where are we going next? J Geophys Res Atmos 124(11):5696–5723
Giorgi F, Marinucci MR, Visconti G (1990) Use of a limited-area model nested in a general circulation model for regional climate simulation over Europe. J Geophys Res Atmos 95(D11):18413–18431
Güttler I, Stepanov I, Branković Č, Nikulin G, Jones C (2015) Impact of horizontal resolution on precipitation in complex orography simulated by the regional climate model RCA3. Mon Weather Rev 143(9):3610–3627
Haarsma RJ, Roberts MJ, Vidale PL, Senior CA, Bellucci A, Bao Q, Chang P, Corti S, Fučkar NS, Guemas V (2016) High resolution model intercomparison project (HighResMIP v1.0) for CMIP6. Geosci Model Dev 9(11):4185–4208
Haarsma R, Acosta M, Bakhshi R, Bretonnière P-A, Caron L-P, Castrillo M, Corti S, Davini P, Exarchou E, Fabiano F (2020) HighResMIP versions of EC-Earth: EC-Earth3P and EC-Earth3P-HR–description, model computational performance and basic validation. Geosci Model Dev 13(8):3507–3527
Hong S-Y, Kanamitsu M (2014) Dynamical downscaling: fundamental issues from an NWP point of view and recommendations. Asia Pac J Atmos Sci 50(1):83–104
Hong S-Y, Lim J-OJ (2006) The WRF single-moment 6-class microphysics scheme (WSM6). Asia Pac J Atmos Sci 42(2):129–151
Hong S-Y, Noh Y, Dudhia J (2006) A new vertical diffusion package with an explicit treatment of entrainment processes. Mon Weather Rev 134(9):2318–2341
Iacono MJ, Delamere JS, Mlawer EJ, Shephard MW, Clough SA, Collins WD (2008) Radiative forcing by long-lived greenhouse gases: calculations with the AER radiative transfer models. J Geophys Res Atmos. https://doi.org/10.1029/2008JD009944
Jang J, Hong S-Y (2014) Quantitative forecast experiment of a heavy rainfall event over Korea in a global model: horizontal resolution versus lead time issues. Meteorol Atmos Phys 124(3):113–127
Jiménez PA, Dudhia J, González-Rouco JF, Navarro J, Montávez JP, García-Bustamante E (2012) A revised scheme for the WRF surface layer formulation. Mon Weather Rev 140(3):898–918
Jin H, Peng MS, Jin Y, Doyle JD (2014) An evaluation of the impact of horizontal resolution on tropical cyclone predictions using COAMPS-TC. Weather Forecast 29(2):252–270
Johnson A, Wang X, Kong F, Xue M (2013) Object-based evaluation of the impact of horizontal grid spacing on convection-allowing forecasts. Mon Weather Rev 141(10):3413–3425
Kim G, Cha DH, Park C, Lee G, Jin CS, Lee DK, Suh MS, Ahn JB, Min SK, Hong SY (2018) Future changes in extreme precipitation indices over Korea. Int J Climatol 38:e862–e874
Kim H, Lee M-I, Cha D-H, Lim Y-K, Putman WM (2019) Improved representation of the diurnal variation of warm season precipitation by an atmospheric general circulation model at a 10 km horizontal resolution. Clim Dyn 53(11):6523–6542
KMA. (2012). Learning from the cases in recent 20 years—top ten heavy rainfall events, Korea Meteorological Administration (in Korean).
Kopparla P, Fischer EM, Hannay C, Knutti R (2013) Improved simulation of extreme precipitation in a high-resolution atmosphere model. Geophys Res Lett 40(21):5803–5808
Lee D-K, Cha D-H (2020) Regional climate modeling for Asia. Geosci Lett 7(1):1–12
Lee J-Y, Kwon M, Yun K-S, Min S-K, Park I-H, Ham Y-G, Jin EK, Kim J-H, Seo K-H, Kim W (2017) The long-term variability of Changma in the East Asian summer monsoon system: a review and revisit. Asia Pac J Atmos Sci 53(2):257–272
Lee M, Cha D-H, Suh M-S, Chang E-C, Ahn J-B, Min S-K, Byun Y-H (2020) Comparison of tropical cyclone activities over the western North Pacific in CORDEX-East Asia phase I and II experiments. J Clim 33(24):10593–10607
Lenderink G, de Vries H, Fowler HJ, Barbero R, van Ulft B, van Meijgaard E (2021) Scaling and responses of extreme hourly precipitation in three climate experiments with a convection-permitting model. Phil Trans R Soc A 379(2195):20190544
Li J, Yu R, Yuan W, Chen H, Sun W, Zhang Y (2015) Precipitation over E ast A sia simulated by NCAR CAM5 at different horizontal resolutions. J Adv Model Earth Syst 7(2):774–790
Li P, Furtado K, Zhou T, Chen H, Li J, Guo Z, Xiao C (2020) The diurnal cycle of East Asian summer monsoon precipitation simulated by the Met Office Unified Model at convection-permitting scales. Clim Dyn 55(1):131–151
Liang J, Tan ML, Hawcroft M, Catto JL, Hodges KI, Haywood JM (2022) Monsoonal precipitation over Peninsular Malaysia in the CMIP6 HighResMIP experiments: the role of model resolution. Clim Dyn 58(9):2783–2805
Lim K-SS, Hong S-Y, Yoon J-H, Han J (2014) Simulation of the summer monsoon rainfall over East Asia using the NCEP GFS cumulus parameterization at different horizontal resolutions. Weather Forecast 29(5):1143–1154
Liu R, Han Z, Wu J, Hu Y, Li J (2017) The impacts of urban surface characteristics on radiation balance and meteorological variables in the boundary layer around Beijing in summertime. Atmos Res 197:167–176
Lucas-Picher P, Argüeso D, Brisson E, Tramblay Y, Berg P, Lemonsu A, Kotlarski S, Caillaud C (2021) Convection-permitting modeling with regional climate models: latest developments and next steps. Wiley Interdiscip Rev Clim Change 12(6):e731
Ma Z, Fei J, Huang X, Cheng X (2012) Sensitivity of tropical cyclone intensity and structure to vertical resolution in WRF. Asia Pac J Atmos Sci 48(1):67–81
Madsen H, Lawrence D, Lang M, Martinkova M, Kjeldsen T (2014) Review of trend analysis and climate change projections of extreme precipitation and floods in Europe. J Hydrol 519:3634–3650
Manabe S, Smagorinsky J, Holloway JL Jr, Stone HM (1970) Simulated climatology of a general circulation model with a hydrologic cycle: III. Effects of increased horizontal computational resolution. Month Weather Rev 98(3):175–212
Mearns L, Giorgi F, McDaniel L, Shields C (1995) Analysis of variability and diurnal range of daily temperature in a nested regional climate model: comparison with observations and doubled CO 2 results. Clim Dyn 11(4):193–209
Meredith EP, Ulbrich U, Rust HW (2020) Subhourly rainfall in a convection-permitting model. Environ Res Lett 15(3):034031
Miguez-Macho G, Stenchikov GL, Robock A (2004) Spectral nudging to eliminate the effects of domain position and geometry in regional climate model simulations. J Geophys Res Atmos. https://doi.org/10.1029/2003JD004495
Moon J, Cha DH, Lee M, Kim J (2018) Impact of spectral nudging on real-time tropical cyclone forecast. J Geophys Res Atmos 123(22):12647–612660
Orlanski I (1975) A rational subdivision of scales for atmospheric processes. Bull Am Meteorol Soc 56:527–530
Otto FE, Philip S, Kew S, Li S, King A, Cullen H (2018) Attributing high-impact extreme events across timescales—a case study of four different types of events. Clim Change 149(3):399–412
Park C, Cha DH, Kim G, Lee G, Lee DK, Suh MS, Hong SY, Ahn JB, Min SK (2020) Evaluation of summer precipitation over Far East Asia and South Korea simulated by multiple regional climate models. Int J Climatol 40(4):2270–2284
Park C, Lee G, Kim G, Cha DH (2021) Future changes in precipitation for identified sub-regions in East Asia using bias-corrected multi-RCMs. Int J Climatol 41(3):1889–1904
Pontoppidan M, Reuder J, Mayer S, Kolstad EW (2017) Downscaling an intense precipitation event in complex terrain: the importance of high grid resolution. Tellus Dyn Meteorol Oceanogr 69(1):1271561
Prein AF, Langhans W, Fosser G, Ferrone A, Ban N, Goergen K, Keller M, Tölle M, Gutjahr O, Feser F (2015) A review on regional convection-permitting climate modeling: demonstrations, prospects, and challenges. Rev Geophys 53(2):323–361

Rauscher SA, O'Brien TA, Piani C, Coppola E, Giorgi F, Collins WD, Lawston PM (2016) A multimodel intercomparison of resolution effects on precipitation: simulations and theory. Clim Dyn 47(7):2205–2218
Sakamoto TT, Komuro Y, Nishimura T, Ishii M, Tatebe H, Shiogama H, Hasegawa A, Toyoda T, Mori M, Suzuki T (2012) MIROC4h—a new high-resolution atmosphere-ocean coupled general circulation model. J Meteorol Soc Jpn Ser II 90(3):325–359
Shi Y, Wang G, Gao X (2018) Role of resolution in regional climate change projections over China. Clim Dyn 51(5):2375–2396
Skamarock WC (2004) Evaluating mesoscale NWP models using kinetic energy spectra. Mon Weather Rev 132(12):3019–3032
Smith S, Vosper S, Field P (2015) Sensitivity of orographic precipitation enhancement to horizontal resolution in the operational Met office weather forecasts. Meteorol Appl 22(1):14–24
Son C, Lee T, Kwon H-H (2017) Integrating nonstationary behaviors of typhoon and non-typhoon extreme rainfall events in East Asia. Sci Rep 7(1):1–9
Tölle MH, Schefczyk L, Gutjahr O (2018) Scale dependency of regional climate modeling of current and future climate extremes in Germany. Theoret Appl Climatol 134(3):829–848
Torma C, Giorgi F, Coppola E (2015) Added value of regional climate modeling over areas characterized by complex terrain—Precipitation over the Alps. J Geophys Res Atmos 120(9):3957–3972
Tripathi OP, Dominguez F (2013) Effects of spatial resolution in the simulation of daily and subdaily precipitation in the southwestern US. J Geophys Res Atmos 118(14):7591–7605
Tselioudis G, Douvis C, Zerefos C (2012) Does dynamical downscaling introduce novel information in climate model simulations of precipitation change over a complex topography region? Int J Climatol 32(10):1572–1578
Uddin MJ, Samad M, Mallik M (2021) Impact of horizontal grid resolutions for thunderstorms simulation over bangladesh using WRF-ARW model. Dhaka Univ J Sci 69(1):43–51
Van Aalst MK (2006) The impacts of climate change on the risk of natural disasters. Disasters 30(1):5–18
Vichot-Llano A, Martinez-Castro D, Giorgi F, Bezanilla-Morlot A, Centella-Artola A (2021) Comparison of GCM and RCM simulated precipitation and temperature over Central America and the Caribbean. Theoret Appl Climatol 143(1):389–402
Volosciuk C, Maraun D, Semenov VA, Park W (2015) Extreme precipitation in an atmosphere general circulation model: impact of horizontal and vertical model resolutions. J Clim 28(3):1184–1205
von Storch H, Langenberg H, Feser F (2000) A spectral nudging technique for dynamical downscaling purposes. Mon Weather Rev 128(10):3664–3673
Wellck RE, Kasahara A, Washington WM, Santo GD (1971) Effect of horizontal resolution in a finite-difference model of the general circulation. Mon Weather Rev 99(9):673–683
Werner M, Langebroek PM, Carlsen T, Herold M, Lohmann G (2011) Stable water isotopes in the ECHAM5 general circulation model: toward high-resolution isotope modeling on a global scale. J Geophys Res Atmos. https://doi.org/10.1029/2011JD015681
Xu Z, Rhoades AM, Johansen H, Ullrich PA, Collins WD (2018) An intercomparison of GCM and RCM dynamical downscaling for characterizing the hydroclimatology of California and Nevada. J Hydrometeorol 19(9):1485–1506
Zheng Y, Alapaty K, Herwehe JA, Del Genio AD, Niyogi D (2016) Improving high-resolution weather forecasts using the Weather Research and Forecasting (WRF) Model with an updated Kain-Fritsch scheme. Mon Weather Rev 144(3):833–860

Publisher's Note